INL/EXT-17-43695

October 2017

Modeling Benchmark for FeCrAl Cladding in the IAEA CRP ACTOF

FeCrAl-C35M Material Models and Benchmark Cases Specifications

Giovanni Pastore
Kyle A. Gamble
Jason D. Hales

INL/EXT-17-43695

Modeling Benchmark for FeCrAl Cladding in the IAEA CRP ACTOF

FeCrAl-C35M Material Models and Benchmark Cases Specifications

Giovanni Pastore
Kyle A. Gamble
Jason D. Hales

October 2017

Idaho National Laboratory
Fuel Modeling and Simulation Department
Idaho Falls, ID 83415

Prepared for the
U.S. Department of Energy
Office of Nuclear Energy
Under U.S. Department of Energy-Idaho Operations Office
Contract DE-AC07-99ID13727

Abstract

This report contains the information necessary to set up fuel performance code calculations for the FeCrAl modeling benchmark in the IAEA ACTOF project. First, we provide a set of models and properties for a selected FeCrAl alloy. Detailed equations and data are given which can be implemented by participants in their codes. Second, we provide standard specifications for the benchmark cases. Proposed cases are relatively simple and cover both LWR normal operating and loss of coolant conditions. Details are given for geometries, input parameters and boundary conditions. To the benefit of the participants, indications on the setup of simulations based on previous experience at INL with the BISON code are also shared. Third, we provide lists of output parameters for code-to-code benchmark comparisons. Relative to previous publications and communications, additional information, data and discussion were added in this report, and corrections were made.

Contents

Introduction

To coordinate and support research on nuclear Accident Tolerant Fuels (ATF) in member countries, the International Atomic Energy Agency (IAEA) sponsored the Coordinated Research Project (CRP) on Analysis of Options and Experimental Examination of Fuels with Increased Accident Tolerance (ACTOF). During the Second Research Coordination Meeting (RCM2) of the ACTOF project in June 2017, a modeling benchmark was proposed as a collaborative activity for project participants. In particular, it was agreed that interested participants would perform fuel performance calculations with their respective fuel performance codes on a set of fuel rod problems with iron-chromium-aluminum (FeCrAl) steel as cladding material. The aim of the work is to perform an initial, meaningful investigation of FeCrAl cladding performance and to compare results from different fuel performance codes. This will bring about important indications about the in-reactor performance of FeCrAl claddings, the current capabilities of nuclear fuel performance codes in modeling FeCrAl, and highlight the important areas of future research. Such concept is along the lines of previous international benchmark exercises (such as the FUMEX series of the IAEA), but with an ATF candidate material being targeted for the simulations. The selected cases are realistic, in order to allow for a meaningful assessment of FeCrAl performance, but simple, as is necessary for initial simulations with a new material and in order to facilitate consistency between the analyses from different participants. This will be a first-time fuel modeling benchmark exercise for ATF and will potentially pave the way for future coordinated research activities in this area.

Idaho National Laboratory (INL) agreed to provide the other ACTOF participants with material properties and models for FeCrAl and detailed standard specifications for the benchmark cases. Preliminary information had been already distributed by INL to the ACTOF participants [1,2]. The present report updates and summarizes the information necessary to perform the FeCrAl fuel performance calculations for the ACTOF modeling benchmark. It is distributed in fulfillment of Action 2.a (for the part on providing material properties for FeCrAl) and Action 3.a (provide FeCrAl modeling input, cases specifications, output format) requested in the Meeting Report of the ACTOF RCM2 [3].

One of the most significant issues in the Fukushima Daiichi accident was the oxidation of Zircaloy that led to a large inventory of hydrogen within the core. Oxidation-resistant FeCrAl alloys have been proposed as light water reactor (LWR) fuel cladding with improved accident tolerance. Oxidation rates for FeCrAl are approximately 1000 times lower than the oxidation rates of Zircaloy [4,5]. In addition, the stiffness of FeCrAl is roughly twice that of Zircaloy [5], while the yield stress is higher by a factor of four for select alloys [4]. While the oxidation characteristics of FeCrAl are a benefit for accident tolerance, the thermal neutron absorption cross section of FeCrAl is about ten times that of Zircaloy. This neutronic penalty necessitates

thinner cladding. This allows for slightly larger pellets to give the same cold gap width in the rod. However, the slight increase in pellet diameter is not sufficient to compensate for the neutronic penalty and enriching the fuel beyond the current 5% limit appears to be necessary [6]. Current estimates indicate that this neutronic penalty will impose an increase in fuel cost of 15-35% [4,5]. In addition to the neutronic disadvantage, it is anticipated that tritium release to the coolant will be larger because the permeability of hydrogen in FeCrAl is about 100 times higher than in Zircaloy [7]. Also, radiation-induced hardening and embrittlement of FeCrAl need to be fully characterized experimentally [8].

For the purpose of a modeling benchmark among different fuel performance codes, it is desirable to agree upon one specific alloy in the first place, and to apply a consistent set of material models and properties in the codes in order to perform meaningful comparisons. FeCrAl alloys for application as nuclear fuel cladding material are currently under development and characterization. Material property data are still limited and mostly from out-of-pile tests. Hence, it is important to select a fairly well characterized alloy with a sufficiently complete set of models and properties available in order to make a meaningful modeling benchmark possible already at this stage.

Many groups of researchers have investigated the behavior of the commercial FeCrAl alloy manufactured by Sandvik AB known as Kanthal APMT^{TM} [9] using INL's fuel performance code BISON [10–12]. However, work has been recently performed at Oak Ridge National Laboratory (ORNL) to develop FeCrAl alloys specifically for nuclear applications [13–17]. This work has ultimately led to development and characterization of the laboratory optimized alloy known as C35M. Based on the experimental data from tests performed at ORNL and at the Halden Reactor, researchers at ORNL and INL have developed empirical models for C35M thermomechanical properties and behavior [2,13,14,16,17]. For areas where C35M experimental data is non-existent, data from the commercial alloy Kanthal APMT^{TM} were used [2]. Models have been developed for thermophysical properties as a function of temperature, thermal and irradiation creep, volumetric swelling, and oxidation. Furthermore, a failure criterion for FeCrAl during loss-of-coolant accident (LOCA) conditions was developed [2]. These models were implemented in INL's code BISON and initial fuel rod calculations with FeCrAl-C35M cladding were performed [2]. As a result of this work, a sufficiently complete set of material models and properties for fuel performance calculations with FeCrAl-C35M is now available. Moreover, this alloy (or similar) is a leading contender to be included in a lead test rod or assembly in a commercial reactor in 2022 as irradiation testing is currently underway in both the Halden Reactor in Norway [17] and the Advanced Test Reactor (ATR) at INL [18].

Therefore, we propose that the C35M alloy is considered for the ACTOF modeling benchmark. With this report we make the set of models and properties available to the ACTOF participants. Furthermore, we provide specifications for the benchmark cases.

Much of the information provided in this report is also found in [2]. However, some updated information is included in this report relative to [2]. In particular:

- An error has been corrected that was present in [2] in the thermal creep correlations (temperature ranges were switched). See Section 1.2, Eqs.1.3 and 1.4.

- We provide the values for the temperature dependent thermal conductivity, specific heat, yield stress and ultimate tensile strength of FeCrAl (Section 1.1). These were not given in [2] (only plots were shown). By interpolating these data, the ACTOF participants can derive the piecewise linear functions for these quantities as used in BISON and implement them in their codes as needed.
- Following a note from Claudia Giovedi in the ACTOF project, we added information on the preliminary instantaneaous plasticity model for FeCrAl used in BISON (Section 1.5), which was not mentioned in [2].
- Per suggestion of Mikhail Veshchunov in ACTOF, the benchmark case for normal operation from [2] was modified by adding a shutdown period at the end of the irradiation history (Section 2.1). The shutdown period may result in increased stresses in the cladding under pellet-cladding mechanical interaction (PCMI) due to the differential thermal contraction of the fuel and cladding during the power decrease.
- Compared to the original normal operation case from [2], a minor modification in the input setting is proposed (using a fuel grain radius of 5 microns, whereas 10 microns were considered originally, which is somewhat high for standard UO_2).
- In general, this report was written with a specific view to the modeling benchmark exercise for ACTOF and contains more detailed and specific information compared to [2]. Hence, for the remaining part of the ACTOF project, it is recommended that the participants refer to this report for setting up the benchmark calculations.

The structure of the report is as follows. FeCrAl-C35M models and properties are described in Section 1. Specifications for the benchmark cases are provided in Section 2. In Section 3 we give indications on the output quantities from the benchmark calculations to be provided by the participants and that will be considered for code-to-code comparisons.

1 Material models and properties for FeCrAl alloy C35M

The C35M alloy is Fe-13Cr-4.5Al + Y with minor alloying additions of molybdenum and silicon. Alloy composition is given in Table 1.1.

Table 1.1: Nominal composition of the ORNL FeCrAl alloy C35M [13].

Fe	Cr	Al	Y	Mo	Si	Remarks
80.15	13	4.5	0.15	2	0.2	Arc-melt + hot-roll

The material models and properties for FeCrAl-C35M provided in this Section were developed at ORNL and INL and may be implemented by other ACTOF participants in their fuel performance codes in view of performing the calculations on the proposed benchmark cases. These fuel performance models have been incorporated into the BISON framework at INL. The correlations provided here benefit from the most recent information on C35M properties from experimental work at ORNL and Halden.

1.1 Thermophysical properties

The temperature dependent Young's modulus and Poisson's ratio of C35M were obtained from Thompson [14] as a function of temperature:

$$E = -5.46 \times 10^{-5} T^2 - 3.85 \times 10^{-2} T + 1.99 \times 10^{2} \tag{1.1}$$

$$\nu = 3.85 \times 10^{-5} T + 2.68 \times 10^{-1} \tag{1.2}$$

where E is the Young's modulus (GPa), ν is Poisson's ratio, and T is the temperature (°C). These equations are valid for temperatures ranging from 25-850°C. (Note that temperature in Eqs. 1.1 and 1.2 is in °C, while K are used for other properties in the following.)

The yield stress and ultimate tensile strength (UTS) of C35M as a function of temperature are illustrated as piecewise functions in Figure 1.1. The plot is adapted from Figure 10 in Yamamoto et al. [13]. At high temperatures it is observed that little ductility remains and failure will occur in a brittle fashion. Irradiation effects on the yield strength and UTS are not taken into account.

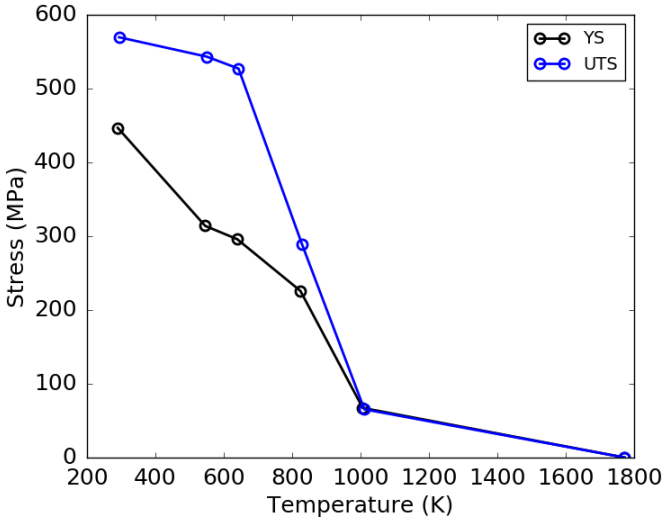

Figure 1.1: Yield stress (YS) and Ultimate Tensile Strength (UTS) as a function of temperature for FeCrAl alloy C35M. The UTS is set to zero at the melting point of C35M.

Table 1.2: Data for yield stress of FeCrAl alloy C35M. Data were digitized from [13]. The value of zero at 1773 K was added in [2] based on observations on other steels.

Temperature (K)	Yield stress (MPa)
291	447
546	314
640	296
825	226
1007	67
1773	0

Yamamoto's data only covers temperatures ranging from about 300 to 1000 K [13]. Based on research by Yano et al. [19] on other ferritic and martensitic steels, there are distinct temperature dependent regions (low, mid, high) of the UTS. In the low temperature region the UTS drops relatively slowly with increasing temperature. In the midrange temperatures there is a rapid decrease in the UTS as temperature increases. The high temperature region results in a slow reduction of the UTS to zero at the melting point. Using these observations on other alloys, an additional data point of a UTS of zero was added to Yamamoto's data at the melting point of C35M (1773 K). Since the yield stress approaches the UTS at the midrange temperatures, the yield stress is also set to zero at the melting point.

For convenience of the ACTOF participants, we also provide here the actual values for yeld stress ad ultimate tensile strength used to derive the piecewise linear functions shown in Figure 1.1 (which were implemented in BISON). Values are collected in Tables 1.2 and 1.3. These values were digitized by Kyle Gamble at INL from Fig. 10 in [13], and are not reported in [2].

Table 1.3: Data for ultimate tensile strength of FeCrAl alloy C35M. Data were digitized from [13]. The value of zero at 1773 K was added in [2] based on observations on other steels.

Temperature (K)	Ultimate Tensile Strength (MPa)
295	569
551	543
644	527
830	289
1012	65
1773	0

The thermal conductivity and specific heat of APMT^{TM} (used in the absence of thermal property data of C35M) are obtained from the datasheet published by the manufacturer Sandvik AB [9]. The values are plotted in Figure 1.2 as a piecewise linear function. The non-monotonic trend of specific heat with temperature is adopted here for conformity with the data but will require further investigation in the future.

For convenience of the ACTOF participants, we also provide here the actual values for thermal conductivity and specific heat used to derive the piecewise linear functions shown in Figure 1.2 (which were implemented in BISON). Values are collected in Tables 1.4 and 1.5. These are not reported in [2].

The coefficient of linear thermal expansion adopted for C35M was taken from the APMT^{TM} datasheet [9]. The mean thermal expansion values are shown in Table 1.6. To obtain the instantaneous thermal expansion coefficient as a function of the temperature, the methodology of

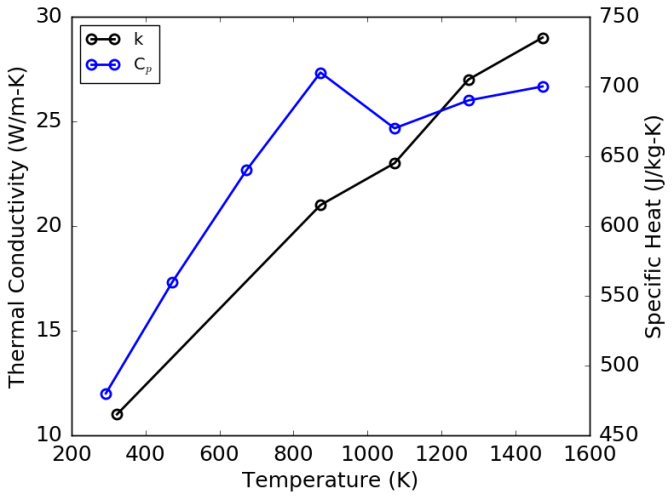

Figure 1.2: Thermal conductivity (k) and specific heat (C_p) piecewise linear functions of temperature for Kanthal APMT^{TM}.

Table 1.4: Data for thermal conductivity of Kanthal APMT^{TM}. Reproduced from [9].

Temperature (K)	Thermal conductivity (W/m-K)
323	11
873	21
1073	23
1273	27
1473	29

Table 1.5: Data for specific heat of Kanthal APMT^{TM}. Reproduced from [9].

Temperature (K)	Specific heat (J/kg-K)
293	480
473	560
673	640
873	710
1073	670
1273	690
1473	700

Table 1.6: Temperature dependent coefficient of thermal expansion (CTE) of Kanthal APMT^{TM}. Reproduced from [9]

Temperature Range (°C)	CTE (μm/m-K)
293 - 523	12.4
293 - 773	13.1
293 - 1023	13.6
293 - 1273	14.7
293 - 1473	15.4

Niffenegger and Reichlin [20] was employed in BISON. Given that the coefficient of linear thermal expansion does not appear to be a strong function of the temperature (Table 1.6), if preferred, also using a constant value in other codes can be acceptable for the modeling benchmark.

1.2 Thermal and irradiation creep

The recommended models for thermal and irradiation creep are given by Terrani et al. [17]. These are based on recent experimental data from in-pile and out-of-pile creep tests performed at Halden and at ORNL. Thermal creep takes the form of the Norton creep law

$$\dot{\varepsilon} = 2.89 \times 10^{-36} \sigma^{5.5} \exp\left(\frac{-29709}{T}\right) \tag{1.3}$$

at temperatures below 873 K. Above 873 K, the correlation proposed by Saunders et al. [21] is used:

$$\dot{\varepsilon} = 5.96 \times 10^{-27} \sigma^{5.5} \exp\left(\frac{-47136}{T}\right) \tag{1.4}$$

where $\dot{\varepsilon}$ is the creep rate (s^{-1}), σ is the effective (von Mises) stress (Pa) and T is the temperature (K). Note that the temperature ranges for Eqs.1.3 and 1.4 are switched in [2] and have been corrected in this report.

The recommended irradiation creep coefficient [17] is 5×10^{-6} per MPa per dpa. By utilizing a conversion factor of 1×10^{25} neutrons/m^2 = 0.9 dpa [22], a correlation for irradiation creep can be derived:

$$\dot{\varepsilon} = 4.5 \times 10^{-31} \sigma \phi \tag{1.5}$$

where σ is the effective stress (MPa) and ϕ is the fast neutron flux (neutrons/m^2-s).

1.3 Volumetric swelling

As a preliminary approach for the swelling of C35M, an upper bound swelling rate provided by Terrani et al. [17] of 0.05% per dpa is considered. Using the same conversion factor as for irradiation creep (1×10^{25} neutrons/m^2 = 0.9 dpa) and integrating over time the volumetric swelling strain is given by:

$$\varepsilon = 4.5 \times 10^{-29} \Phi \tag{1.6}$$

where and Φ is the fast neutron fluence (neutrons $m/^2$).

Also, the incubation behavior of swelling is not considered at this time, and should be included in the future as relevant data become available.

1.4 Oxidation kinetics

One of the advantages of FeCrAl alloys over zirconium-based alloys is their increased oxidation resistance. The model implemented in BISON for FeCrAl-C35M waterside oxidation is based on recent autoclave experiments completed by Terrani et al. [16]. The experiments were conducted at normal operating temperatures 330°C and 290°C for PWR and BWR, respectively. Parabolic oxide growth kinetics govern the mass gain as a result of the formation and growth of the chromium-rich chromite ($FeCr_2O_4$) layer:

$$w = k\sqrt{t} \tag{1.7}$$

where k is the parabolic oxidation rate constant (mg/cm^2-h$^{1/2}$) and t is the time (h). The thickness of the chromite layer is then given by:

$$\delta = \frac{w}{\rho_{ox}} \tag{1.8}$$

where ρ_{ox} is assumed to be the density of oxygen in chromite (1440 kg/m^3) [16].

The parabolic rate constants used from [16] in the BISON model are 3.96×10^{-3} and 4.51×10^{-4} mg/cm^2-h$^{1/2}$ for PWR and BWR-NWC coolant conditions, respectively. These correspond to the FeCrAl alloy with composition of Fe-13Cr-4Al which most closely represents the C35M alloy of interest in this work. Note that these rate constants are independent of temperature. As new data is becomes available the temperature dependence of the oxidation rate constant will be taken into account. It should be noted that in addition to the formation of an oxide scale, additional metal in FeCrAl alloys will dissolve into the water, which results in a further reduction of the overall cladding thickness [16]. This dissolution process does not occur in zirconium-based alloys. It is neglected in the BISON model at this time.

1.5 Instantaneous plasticity

Cladding plasticity in BISON is taken into account by means of an isotropic von Mises plasticity model (e.g., [23]). In the absence of specific information on plastic behavior for FeCrAl alloys at this time, we adopt a simplified treatment that considers an hardening slope of 2.5×10^9 Pa after the yields strength is exceeded. For the calculation of the yield stress, see Section 1.1.

1.6 Burst failure criterion

A failure model for FeCrAl under loss of coolant accident conditions was developed at INL [2]. The model consists of an overstress criterion, which establishes that cladding failure occurs when the local hoop stress exceeds a limiting burst stress. This concept is analogous to overstres criteria used for burst failure of Zircaloy under loss-of-coolant conditions [24,25]. The burst stress varies as a function of temperature and is derived from the failure behavior measured in recent out-of-pile FeCrAl cladding burst tests completed at ORNL by Massey et al. [15]. In the experiments, the specimens were 30 cm long, with inner/outer diameter of 8.73/9.5 mm (385 mm thick) cladding tubes filled with zirconia pellets. The rods were internally pressurized with helium and exposed to continually flowing steam at atmospheric pressure (0.1 MPa) on their outer surface. The initial pres- sure of each rod was different. Using an infrared furnace the temperature of the cladding was ramped from 300 C to 1200 C at a rate of 5 C/s, held for 3 min, ramped down to 800 C at a rate of 5 C/s, before being quenched with water. The increasing temperature caused the internal pressure of the tube to rise until failure of the tube occurred. The internal pressure was measured with a pressure transducer and the cladding surface temperature was determined with at least three Type-S thermocouples [15]. To the best of our knowledge,

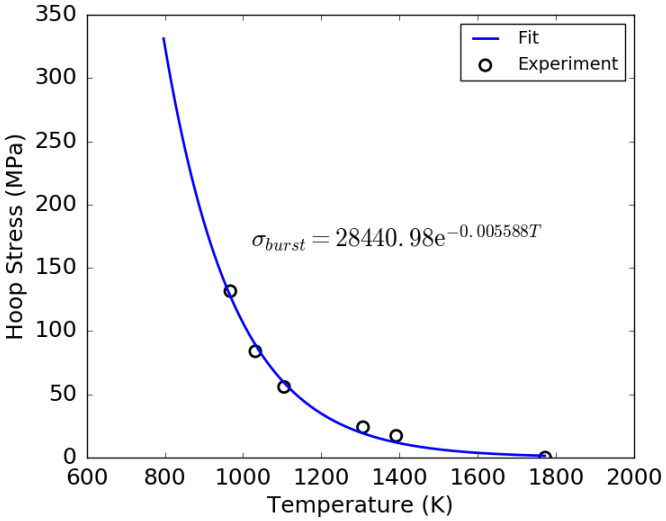

Figure 1.3: Exponential fit for limiting burst stress.

Massey et al.'s are the only experimental data available on burst failure behavior of FeCrAl claddings under LOCA conditions.

From the measured tube pressures, data were given in [15] in terms of hoop stress according to temperature at burst failure. Using a least squares methodology, a best fit to the data is performed to obtain a correlation for burst (hoop) stress as an exponential function of temperature. An additional point of zero hoop stress at the melting point (1773 K) was used. An illustration of the experimentally derived stress data, and best fit equation, is shown in Figure 1.3. It is also noted that at low temperatures the UTS provides a conservative failure criterion [2]. Therefore, the developed burst stress correlation is given by [2]:

$$\sigma_{burst} = \begin{cases} \text{Ultimate Tensile Strength}, & \text{for } T \leq 796.8 \text{ K} \\ 28440.98e^{-0.005588T}, & \text{for } T > 796.8 \text{ K} \end{cases} \tag{1.9}$$

where T is temperature. The exponential decay of the burst stress at high temperature is encouraging as it matches the functional form proposed by Erbacher et al. [24] for Zircaloy claddings (excluding the oxygen content contribution). It should be emphasized that the burst data from Massey et al. [15] is for ORNL first generation FeCrAl alloys whereas C35M is a second generation FeCrAl alloy. The first generation alloys had large grain sizes and are expected to be weaker than second generation alloys such as C35M [13]. In the absence of specific data for the bust behavior of C35M, the burst criterion described above is used in BISON and is expected to provide conservative burst failure predictions for C35M.

1.7 Concluding remarks

The material models and properties for FeCrAl-C35M provided in this report may be implemented by other ACTOF participants in their fuel performance codes in view of performing the calculations on the proposed benchmark cases. These cases are described in Section 2. Because the benchmark case for normal operating conditions consists of a FeCrAl cladded fuel rodlet with UO_2 fuel, UO_2 models are applied in the calculations along with FeCrAl models. Also, fuel-cladding thermal and mechanical interactions need to be considered. Finally, performing calculations for analogous cases with Zircaloy-4 cladding instead of FeCrAl cladding is suggested in order to obtain useful comparisons and additional insight. The models used in INL's code BISON for UO_2 fuel, Zircaloy-4 cladding and fuel-to-cladding gap are summarized in previous publications [26–30]. Nevertheless, for these standard materials and fuel performance aspects, it remains understood that other participants will apply their own codes' models. Differences in the results from different codes will then be investigated following the benchmark comparisons.

However, while different codes may use different material and behavioral models, for code-to-code comparisons to be meaningful the same specifications for the benchmark cases (geometry, power histories, boundary conditions) should be adopted by all participants in a consistent way. The standard specifications for the benchmark cases are proposed by INL and are provided in Section 2.

2 Standard specifications for the benchmark cases

In this section, details are given of the test cases for benchmark comparisons. Proposed cases are relatively simple and include a short PWR fuel rod irradiated under idealized normal operating conditions and some cladding-only cases for prototypic loss-of-coolant conditions. These cases have been already used for initial calculations at INL with the BISON code [2]. Simulations would be performed considering FeCrAl as cladding material. Performing additional calculations for analogous cases with Zircaloy-4 for comparison is also suggested. Specifications are given here for both the FeCrAl cases and the corresponding, as far as possible consistent, Zircaloy-4 cases.

Note that the specifications proposed in this section may not necessarily be the final ones; if discussions within ACTOF or the experience of participants in performing the calculations will lead to suggestions for modifications, these can be considered. However, it is suggested that the main settings and concepts are maintained, given the limited time frame for completing the modeling benchmark (with the end of ACTOF being set before the end of 2018).

2.1 Normal operating conditions

The proposed benchmark case for LWR normal operating conditions is a simple, idealized test case of a short (10-pellet) rod with typical PWR specifications irradiated under steady-state conditions. The idea is to analyze FeCrAl cladding behavior during the irradiation, and to compare with Zircaloy-4 behavior. UO_2 fuel is considered in either case.

The assumed geometry, shown in Figure 2.1, includes a UO_2 fuel stack of 118.6 mm height, FeCrAl (or Zircaloy-4) cladding, an initial 80 μm pellet-cladding radial gap, and plena. Note that, although Figure 2.1 shows a discrete-pellet mesh, a smeared mesh which treats the fuel column as a monolithic stack was considered for the BISON simulations so far.

To enable comparisons between the two systems (UO_2/FeCrAl and UO_2/Zircaloy-4) the initial rodlet diameter (cladding outer diameter) and fuel-to-cladding gap are the same. The cladding thickness varied depending upon the cladding material used. For the FeCrAl cases the cladding was thinner to accommodate the neutronic penalty introduced by the increased neutron absorption cross-section. This allows for slightly larger pellets to give the same cold gap width in the rod. The cladding thicknesses for both Zircaloy-4 and FeCrAl were obtained from [15]. FeCrAl cladding thickness is based on the neutronic analysis from [6]. The BISON model also included

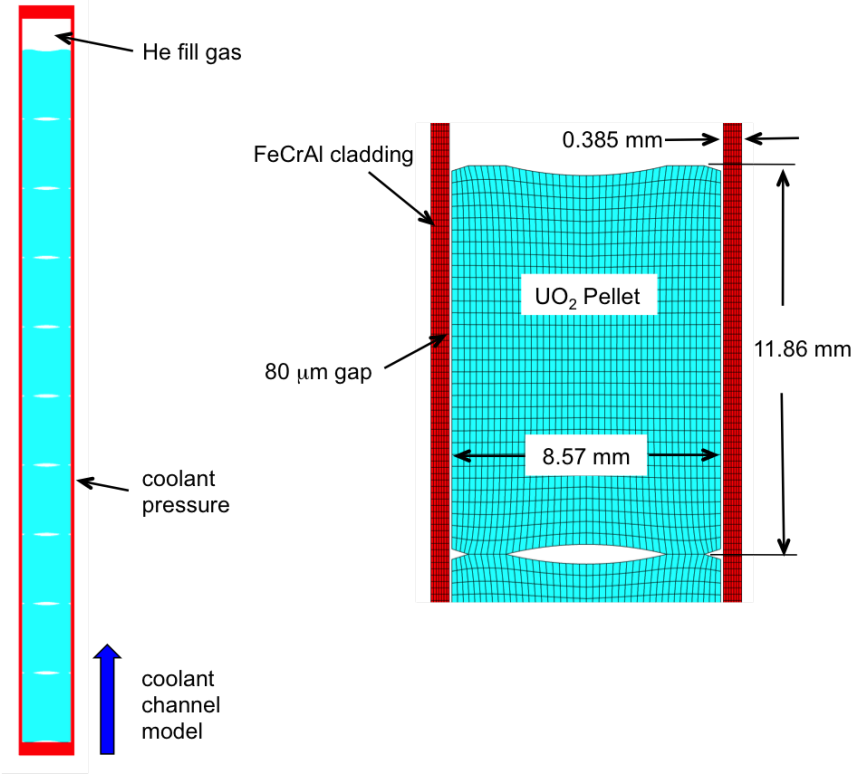

Figure 2.1: Geometry and materials for the FeCrAl normal operation benchmark case. Although the figure shows a discrete-pellet mesh, a smeared fuel column mesh was considered for the baseline BISON simulations. Note that cladding thickness and pellet diameter are different for Zircaloy-4 cladding.

a small lower plenum. As not every fuel performance code allows for a lower plenum, this can be made up by adjusting the upper plenum height. It is just recommened to be consistent in terms of total rod free volume (also provided in Table 2.1).

For completeness of information: In the BISON calculation we consider a lower end plug and an upper end plug of 2.24 and 2.16 mm height, respectively. These are not necessarily realistic but it was verified that the analysis is not sensitive to dimensions of plugs for the purposes of interest here. Some codes do not consider plugs explicitly and consistency among codes for dimensions of end plugs is not required for the benchmark calculations.

The linear heat rate history for this normal operation case consists of a linear ramp from 0 to 25 kW/m over 3 hours, a hold at constant power for about 4 years (precisely, 35037 hours, which makes it 4 years from startup), and a final power shutdown over 3 hours (Figure 2.2). Hence, the power variations (startup and shutdown) are considered to occur at a power ramp rate of about 0.14 kW/m-min. A flat axial profile is assumed for the rodlet. The same power history is used for either the FeCrAl and Zircaloy-4 case. In reality, rod power will be different for FeCrAl cladded rods relative to Zircaloy due to the increased fuel loading and enrichment necessary to overcome the neutronic penalty. Nevertheless, the comparisons obtained using a simplified power history

Table 2.1: Specifications for the normal operation benchmark case. Both the UO_2/Zircaloy-4 and the UO_2/FeCrAl cases are included.

	UO_2/Zircaloy-4 Rodlet	UO_2/FeCrAl Rodlet
Number of pellets	10	10
Pellet length (mm)	11.86	11.86
Pellet inner diameter (mm)	0	0
Pellet outer diameter (mm)	8.19	8.57
Chamfers, dishes	no	no
Initial fuel density (%TD)	95	95
Initial fuel density (kg/m^3)	10431	10431
Initial fuel enrichment (%)	5	5
Initial fuel grain radius (3D) (μm)	5	5
Radial gap width (μm)	80	80
Initial fill gas	He	He
Initial fill pressure (MPa)	2	2
Cladding inner diameter (mm)	8.35	8.73
Cladding thickness (mm)	0.575	0.385
Cladding outer diameter (mm)	9.5	9.5
Upper plenum height (mm)	26	26
Lower plenum height (mm)	1	1
Total free volume (cc)	1.725	1.874
Total rodlet length (incl. plugs) (mm)	150	150
Coolant inlet mass flux (kg/m^2-s)	3800	3800
Coolant inlet temperature (K)	580	580
Coolant pressure (MPa)	15.5	15.5
Pin pitch (mm)	12.6	12.6

can provide valuable insight into the response of FeCrAl cladded rods under normal operating reactor conditions. Note that a 25 kW/m power level is relatively high compared to typical average operating power for PWR rods, and a 4-year irradiation is relatively long. These choices were made to analyze cladding behavior including the effect of prolonged PCMI driven by fuel thermal expansion and gaseous swelling. Rod power as well as duration of the irradiation could be varied (e.g., see FUMEX-II simplified cases [31]) if benchmark comparisons for different conditions are of interest.

In the BISON simulations, thermal (convective) boundary conditions are applied using a single subchannel coolant channel model with the coolant conditions provided in Table 2.1. The bottom of the rodlet is assumed to be the coolant channel inlet.

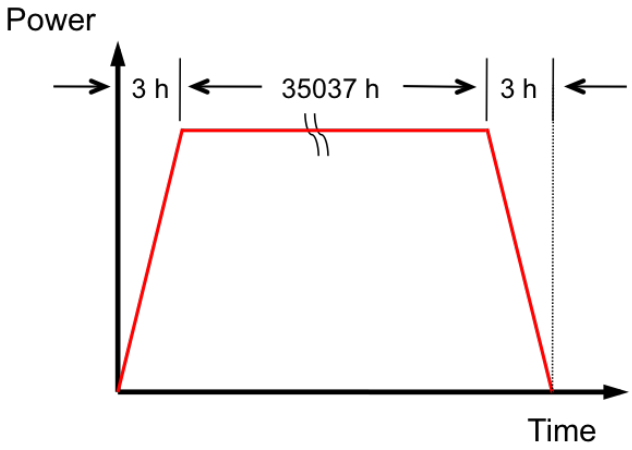

Figure 2.2: Schematic of power history for the normal operation benchmark case. Steady-state linear power level is 25 kW/m.

2.2 Loss of coolant conditions

The initial INL study [2] also covered loss-of-coolant accident conditions. It is proposed that loss-of-coolant conditions are considered also for the ACTOF modeling benchmark. However, it is recommended that calculations are focused first on the normal operation case (Section 2.1), which will allow for testing the basic FeCrAl capabilities in the codes. Then, LOCA calculations can be performed, to exercise models for high-temperature FeCrAl behavior, such as high-temperature creep and burst failure criteria. Comparisons to Zircaloy behavior under analogous conditions is also of interest. Note that for the proposed cases experimental data for Zircaloy-4 are available, so we can compare directly to the experimental data rather than performing corresponding Zircaloy-4 simulations (see below).

For the benchmark cases for loss of coolant conditions, we propose to consider the conditions of the separate-effects experimental tests PUZRY from AEKI [32]. These are cladding-only ballooning and burst tests performed on Zircaloy-4 tubes under well defined experimental conditions. In these experiments, tube samples were investigated in a resistance furnace providing isothermal conditions in the temperature range of 973-1473 K. The inner pressure of the test tube was increased linearly until the burst of the sample. The specimens were 50 mm long with inner/outer diameters of 9.3/10.75 mm, respectively. The specimen was placed in a quartz test tube filled with inert argon gas, and heated up in an electrical furnace. The pressure of the inert gas in the quartz tube was kept constant at 0.1 MPa. After an approximately 1000 s heat-up period, the sample was pressurized with argon gas at a constant pressurization rate. Pressurization rates between 7×10^{-4} and 2.6×10^{-2} MPa/s were tested. The effect of corrosion on the mechanical performance of Zircaloy-4 cladding was not investigated. The schematic drawing of the specimen is reported in Figure 2.3.

In total, the experiment included 31 tests, but for the present modeling benchmark we propose

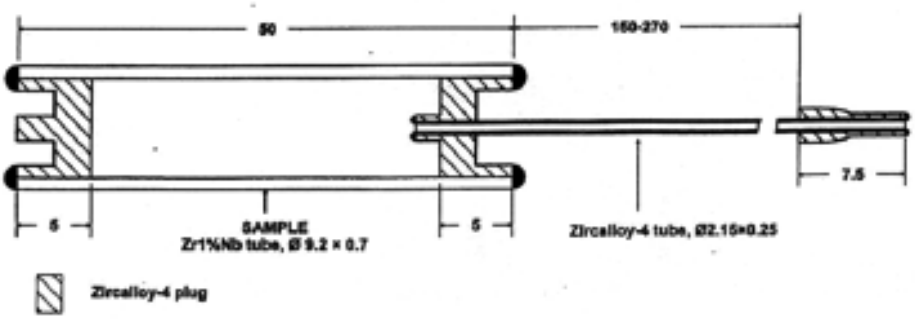

Figure 2.3: Drawing of the tube specimen for the cladding-only burst tests PUZRY [32]. Note that Zircaloy-4 tubes were used for the tests.

to consider only a subset of these (see below). Applying the known experimental conditions to FeCrAl rodlets of appropriate thicknesses, FeCrAl behavior under prototypical loss of coolant transient conditions can be investigated. The reasons for the choice of the PUZRY cases are:

- Considering separate-effects, cladding-only tests with well defined experimental conditions (temperature, pressure histories) avoids complexities associated with integral fuel rod behavior (thermal and mechanical analyses of fuel and cladding, fuel-cladding interactions). Isolating cladding behavior is thought to be ideal for testing codes' capabilities and performing a first modeling benchmark for a new material. Integral fuel rod cases can be considered for a future benchmark at a later stage (e.g., ACTOF-II).
- Among the separate-effects experimental databases available, the PUZRY tests are priority cases also in the IAEA CRP on Fuel Modeling under Accident Conditions FUMAC. Hence, (i) there is previous experience in modeling the experimental conditions of the PUZRY tests, which could be leveraged by the ACTOF participants, and (ii) having the same cases considered by modelers in two CRPs may lead to further useful comparisons and communication between the projects.

Because the PUZRY experiments were performed in inert gas (Ar) atmosphere, they do not allow for investigating the effect of oxidation. This can be appropriate for this first modeling benchmark because, to the best of our knowledge, models for the high-temperature oxidation of FeCrAl are not yet available. In a future perspective, simulations of loss of coolant conditions considering an oxidizing environment can be carried out.

The actual PUZRY experiments were performed on Zircaloy-4 tubes. For the ACTOF benchmark calculations we consider FeCrAl material instead, however, we use the experimental conditions and geometry of the PUZRY tests. The exception is the considered cladding thickness that will be lower in order to perform realistic simulations with FeCrAl. In particular, the recommended cladding thickness for FeCrAl is 385 μm (same as with the normal operation benchmark case, see Section 2.1). The results from the diferent codes will then be compared based on calculations with this cladding thickness. Specifications for the ACTOF proposed benchmark cases for loss of coolant conditions are summarized in Table 2.2.

Table 2.2: Specifications for the LOCA benchmark cases.

Tube specimen alloy	FeCrAl
Inner radius (mm)	4.65
Thickness (μm)	385
Length (mm)	50
End plug length (mm)	5
Atmosphere	Ar
Outer pressure (MPa)	0.1

Table 2.3: Conditions of the 6 PUZRY experiments selected as LOCA benchmark cases [32].

Rod number	Temperature (K)	Pressure ramp rate (MPa/s)
8	1274.15	0.00763
10	1375.75	0.00710
12	1470.85	0.00723
18	1173.35	0.01151
26	971.55	0.01193
30	1073.55	0.02630

We propose to limit the benchmark calculations to six cladding tests from the PUZRY series. The choice is based upon the selected cases for FUMAC [33]. Temperature and pressure conditions for the selected tests are summarized in Table 2.3.

The data provided above should enable ACTOF participants to set up their calculations. These cases were already modeled by INL with the BISON code [2]. To the benefit of the ACTOF modelers, we also share some details of the BISON setup adopted for the calculations, in case they can be useful to other participants:

- Finite-element 2D axisymmetric models of the cladding tubes were used.
- Taking advantage of the symmetry of the problem, only the lower half of the heated cladding length was modeled.
- The end plugs restrain the cladding radial strain and need to be considered in the simulations. In the BISON model, end plugs were considered by preventing radial motion (i.e., applying zero radial displacement boundary conditions) to the tube inner surfaces in correspondence of the plugs. These correspond to the 5 mm end sections of the cladding (see Fig 2.3). Note that only one plug is explicitly included in the BISON model as we consider only the lower half of the tube (the other half of the sample is accounted for by symmetry).
- Time-dependent pressures were simulated by Dirichlet pressure boundary conditions applied to the tube inner and outer walls.

- The furnace heating was simulated by a Dirichlet temperature boundary condition applied to the tube outer wall. In the PUZRY database [32], tubes temperature profiles along the axial direction are not given. However, applying a perfectly uniform temperature axially would lead to a distributed ballooning along the tube, while several experiments showed localized ballooning with maximum strain and burst occurring near the tube's mid-plane. This can be interpreted as associated with axial temperature variations that, albeit small, lead to significant strain axial variations by virtue of the strong (exponential) temperature dependence of the creep rate. To account for this, we included a slight axial temperature variation in the BISON simulations. (Note that much lower or negligible creep is expected for FeCrAl relative to Zircaloy-4 [15]. However, accounting for temperature peaking is necessary to reproduce localized burst.) Within FUMAC, Katalin Kulacsy communicated that axial temperature variations of 5-6 K along the central 50 mm section of the furnace can be expected, based on measurments performed in another furnace [34]. On this base, in the BISON simulations we applied a linear temperature profile (simplest possibility in absence of detailed indications) with the maximum temperature applied at the mid-plane (consistent with experimental observations of localized ballooning close to the mid-plane of the specimen). The overall (tube end to tube mid-plane) variation was made equal to 6 K, with the average (tube quarter-length) temperature being equal to the experimental value (Table 2.3).
- Prior to the pressure transient, we considered the initial heat-up period by applying atmospheric (0.1 MPa) pressure to both sides of the tube and ramping the temperature up from ambient (300 K) to the test temperature (Table 2.3) over 1000 s. The inner pressure transient from 0.1 MPa at the experimental rate (Table 2.3) was applied afterwards, under isothermal conditions. Outer tube pressure was kept constant at 0.1 MPa.

A complication arises with respect to the potential comparisons to the Zircaloy-4 experimental data from the corresponding PUZRY experiments. In the experiments, the Zircaloy-4 cladding thickness was 725 μm which is 1.26 times greater than the Zircaloy-4 thickness of 575 μm suggested by [16] that is used in the normal operation simulations (Section 2.1). These thicker claddings are likely representative of older designs. Because cladding thickness importantly affects the resistance to burst, in order to compare the burst performance of 385 μm thick FeCrAl tubes to equivalent Zircaloy-4 tubes, ideally, data from Zircaloy tubes with lower thicknesses would be needed (e.g., 575 μm as used in the normal operation case, Section 2.1). However, since the available (PUZRY) data refer to 725 μm thick Zircaloy-4 tubes, to make consistent comparisons we propose to perform additional FeCrAl simulations with a higher thickness. In particular, considering a 483.43 μm thick cladding is proposed, because it is 1.26 times greater than the thickness used for FeCrAl in the baseline calculations (385 μm). For examples of applications of this approach and comparisons of FeCrAl and Zircaloy-4 burst behavior based on the same PUZRY cases proposed here, see the work of Gamble et al. [2]. For convenience of the ACTOF participants, the Zircaloy-4 experimental data for the 6 considered PUZRY cases are reported in Table 2.4.

Calculations with the reference FeCrAl tube thickness of 385 μm should be the priority as they will represent the basis for codes benchmark comparisons. Additional calculations with 483.43

Table 2.4: Experimental data (Zircaloy-4) for the 6 PUZRY experiments selected [32]. Time to burst is intended from the beginning of the transient.

Rod number	Time to burst (s)	Burst pressure (MPa)	Maximum hoop strain at burst (%)
8	116.7	0.890	80.37
10	92.0	0.653	72.76
12	80.0	0.578	71.62
18	233.7	2.689	74.29
26	888.8	10.605	100.97
30	275.7	7.251	104.28

μm thick cladding would be performed subsequently for the purpose of adding comparisons to Zircaloy behavior.

Ideally, for the benchmark only one case should be considered initially, so that any initial issues with the simulations can be discussed and first comparisons can be performed on the same case, thus facilitating collaboration. The choice of this 'priority' case is essentially arbitrary. We propose that every participant considers the PUZRY-8 case before any other for the LOCA calculations. Other cases would be considered only at a later stage (if time allows) once both the normal operation case and the PUZRY-8 cases are completed.

3 Output format for code-to-code comparisons

Calculated quantities proposed for comparisons of results from the participants within the ACTOF modeling benchmark are listed in Sections 3.1 and 3.2 for the normal operation and LOCA cases, respectively. The lists are not necessarily final or comprehensive and proposals are welcome for additional comparisons.

Proposed format for the results is MS Excel–readable files. It is recommended to include labels and units as well as comments to make the provided data clearly understandable. INL offers to eventually collect the results and produce comparisons for the ACTOF final report.

3.1 Normal operating conditions calculations

For the normal operation case (Section 2.1), figures of merit proposed for code-to-code comparisons are time evolution histories of:

- Hoop strain at cladding inner and outer surfaces.
- Hoop stress at cladding inner and outer surfaces.
- Fuel-cladding radial gap width.
- Oxide layer thickness.
- Fuel centerline temperature.
- Rod inner pressure.
- Fission gas release.

Note that cladding hoop strain and stress, gap width, oxide thickness and fuel centerline temperature are local values at an axial location corresponding to the mid-plane of the fuel stack.

3.2 Loss of coolant conditions calculations

For the LOCA case(s) (Section 2.2), figures of merit proposed for code-to-code comparisons are:

- Time to cladding burst failure.
- Cladding inner pressure at burst.
- Hoop strain (at cladding outer surface and peak axial location) at the time of burst.
- Hoop strain (at cladding outer surface and peak axial location) as a function of time.

Acknowledgments

This work was funded by the US DOE Nuclear Energy Advanced Modeling and Simulation program. The manuscript has been authored by a contractor of the U.S. Government under Contract DE-AC07-05ID14517. Accordingly, the U.S. Government retains a non-exclusive, royalty free license to publish or reproduce the published form of this contribution, or allow others to do so, for U.S. Government purposes.

The work fits in the framework of the Coordinated Research Project (CRP) on Analysis of Options and Experimental Examination of Fuels with Increased Accident Tolerance (ACTOF) of the IAEA and benefited from the discussion within the CRP. Travel funding from IAEA is also acknowledged. INL participates in ACTOF under the CRADA agreement 16-CRP-01.

Katalin Kulacsy (Hungarian Academy of Sciences) is acknowledged for making the PUZRY experimental data available to the ACTOF project.

References

[1] G. Pastore. Fuel rod test case for ATF modeling benchmark within ACTOF, December 2016. Available on the ACTOF website, https://nucleus.iaea.org/sites/nefw-projects/crpactof/SitePages/Home.aspx.

[2] K.A. Gamble, T. Barani, D. Pizzocri, J.D. Hales, K.A. Terrani, and G. Pastore. An investigation of FeCrAl cladding behavior under normal operating and loss of coolant conditions. *Journal of Nuclear Materials*, 491:55 – 66, 2017.

[3] P. Xu. Meeting Report of the 2nd Research Coordination Meeting related to the IAEA Coordinated Research Project T12030 on Analysis of Options and Experimental Examination of Fuels for Water-Cooled Reactors with Increased Accident Tolerance (ACTOF). Technical report, International Atomic Energy Agency, 2017.

[4] R. E. Stachowski, R. B. Rebak, W. P. Gassmann, and J. Williams. Progress of GE development of accident tolerant fuel FeCrAl cladding. In *Proceedings of TopFuel*, Boise, ID, USA, 2016.

[5] K. A. Terrani, S. J. Zinkle, and L. L. Snead. Advanced oxidation-resistant iron-based alloys for LWR fuel cladding. *Journal of Nuclear Materials*, 448:420–435, 2014.

[6] N. M. George, K. A. Terrani, J. Powers, A. Worrall, and I. Maldonado. Neutronic analysis of candidate accident-tolerant cladding concepts in pressurized water reactors. *Annals of Nuclear Energy*, 75:703–712, 2015.

[7] X. Hu, K. A. Terrani, B. D. Wirth, and L. L. Snead. Hydrogen permeation in FeCrAl alloys for LWR cladding application. *Journal of Nuclear Materials*, 461:282–291, 2015.

[8] K. G. Field, R. Howard, and Y. Yamamoto. Experimental plan and irradiation target design for FeCrAl embrittlement screening tests conducted using the high flux isotope reactor. Technical Report ORNL/TM-2015/311, Oak Ridge National Laboratory, 2015.

[9] Kanthal APMT (Tube) Datasheet, 2012. http://kanthal.com/en/products/material-datasheets/tube/kanthal-apmt/.

[10] X. Wu, T. Kozlowski, and J.D. Hales. Neutronics and fuel performance evaluation of accident tolerant FeCrAl cladding under normal operation conditions. *Annals of Nuclear Energy*, 85:763–775, 2015.

[11] J. Galloway and C. Unal. Accident-Tolerant-Fuel Performance Analysis of APMT Steel Clad/UO_2 Fuel and APMT Steel Clad/UN-U_3Si_5 Fuel Concepts. *Nuclear Science and Engineering*, 182:523–537, 2015.

[12] R. Sweet, N. George, K. Terrani, and B. Wirth. BISON fuel performance analysis of FeCrAl cladding with updated properties. Technical Report ORNL/TM-2016/475, Oak Ridge National Laboratory, 2016.

[13] Y. Yamamoto, B.A. Pint, K.A. Terrani, K.G. Field, Y. Yang, and L.L. Snead. Development and property evaluation of nuclear grade wrought FeCrAl fuel cladding for light water reactors. *Journal of Nuclear Materials*, 467:703–716, 2015.

[14] Z. T. Thompson, K. A. Terrani, and Y. Yamamoto. Elastic Modulus Measurement of ORNL ATF FeCrAl Alloys. Technical Report ORNL/TM-2015/632, Oak Ridge National Laboratory, October 2015. Available at http://info.ornl.gov/sites/publications/files/Pub59679.pdf.

[15] C. P. Massey, K. A. Terrani, S. N. Dryepondt, and B. A. Pint. Cladding burst behavior of Fe-based alloys under LOCA. *Journal of Nuclear Materials*, 470:128–138, 2016.

[16] K.A. Terrani, B.A. Pint, K.A. Unocic, Y. Yang, C.M. Silva, H.M. Meyer III, and R.B. Rebak. Uniform corrosion of FeCrAl alloys in LWR coolant environments. *Journal of Nuclear Materials*, 479:36–47, 2016.

[17] K. A. Terrani, T. M. Karlsen, and Y. Yamamoto. Input correlations for irradiation creep of FeCrAl and SiC based on in–pile Halden test results. Technical Report ORNL/TM-2016/191, ORNL, May 2016. Available at http://info.ornl.gov/sites/publications/files/Pub62748.pdf.

[18] K.G. Field, K. Barrett, Z. Sun, and Y. Yamamoto. Submission of FeCrAl feedstock for support of AFC ATR-2 irradiations. Technical Report ORNL/TM-2016/426, 2016.

[19] Y. Yano, T. Tanno, Y. Sekio, H. Oka, S. Ohtsuka, T. Uwaba, and T. Kaito. Tensile properties and hardness of two types of 11Cr-ferritic/martensitic steel after aging up to 45,000 h. *Nuclear Materials and Energy*, 000:1–7, 2016.

[20] M. Niffenegger and K. Reichlin. The proper use of thermal expansion coefficients in finite element calculations. *Nuclear Engineering and Design*, 243:356–359, 2012.

[21] S. R. J. Saunders, H. E. Evans, M. Li, D. D. Gohil, and S. Osgerby. Oxidation growth stresses in an alumina-forming ferritic steel measured by creep deflection. *Oxidation of Metals*, 48:189–200, 1997.

[22] K. G. Field, X. Hu, K. C. Littrell, Y. Yamamoto, and L. L. Snead. Radiation tolerance of neutron-irradiated model Fe-Cr-Al alloys. *Journal of Nuclear Materials*, 465:746–755, 2015.

[23] F. Dunne and N. Petrinic. *Introduction to Computational Plasticity*. Oxford University Press, Oxford, 2005.

[24] F. J. Erbacher, H. J. Neitzel, H. Rosinger, H. Schmidt, and K. Wiehr. Burst criterion of Zircaloy fuel claddings in a loss-of-coolant accident. In *Zirconium in the Nuclear Industry, Fifth Conference, ASTM STP 754, D.G. Franklin Ed.*, pages 271–283. American Society for Testing and Materials, 1982.

[25] V. Di Marcello, A. Schubert, J. van de Laar, and P. Van Uffelen. The TRANSURANUS mechanical model for large strain analysis. *Nuclear Engineering and Design*, 276:19–29, 2014.

[26] R. L. Williamson, J. D. Hales, S. R. Novascone, M. R. Tonks, D. R. Gaston, C. J. Permann, D. Andrs, and R. C. Martineau. Multidimensional multiphysics simulation of nuclear fuel behavior. *Journal of Nuclear Materials*, 423:149–163, 2012.

[27] J. D. Hales, R. L. Williamson, S. R. Novascone, G. Pastore, B. W. Spencer, D. S. Stafford, K. A. Gamble, D. M. Perez, R. J. Gardner, and W. Liu. BISON theory manual: The equations behind nuclear fuel analysis. Technical Report INL/EXT–13–29930, Rev. 1, Idaho National Laboratory, ID, USA, 2014.

[28] G. Pastore, L. P. Swiler, J. D. Hales, S.R. Novascone, D. M. Perez, B. W. Spencer, L. Luzzi, P. Van Uffelen, and R. L. Williamson. Uncertainty and sensitivity analysis of fission gas behavior in engineering-scale fuel modeling. *Journal of Nuclear Materials*, 456:398–408, 2015.

[29] R.L. Williamson, K.A. Gamble, D.M. Perez, S.R. Novascone, G. Pastore, R.J. Gardner, J.D. Hales, W. Liu, and A. Mai. Validating the BISON fuel performance code to integral LWR experiments. *Nuclear Engineering and Design*, 301:232 – 244, 2016.

[30] T. Barani, E. Bruschi, D. Pizzocri, G. Pastore, P. Van Uffelen, R.L. Williamson, and L. Luzzi. Analysis of transient fission gas behaviour in oxide fuel using BISON and TRANSURANUS. *Journal of Nuclear Materials*, 486:96–110, 2017.

[31] IAEA. Fuel Modelling at Extened Burnup (FUMEX-II): Report of a Coordinated Research Project 2002-2007. Technical Report IAEA-TECDOC-1687, International Atomic Energy Agency, 2012.

[32] E. Perez-Feró, Z. Hózer, T. Novotny, G. Kracz, M. Horváth, I. Nagy, A. Vimi, A. Pintér-Csordás, Cs. Győri, L. Matus, L. Vasáros, P. Windberg, and L. Maróti. Experimental Database of E110 Claddings under Accident Conditions. Technical Report EK-FRL-2012-255-01/02, Centre for Energy Research, Hungarian Academy of Sciences, Budapest, Hungary, May 2013.

[33] J. Zhang and M. Veshchunov. Status update of the IAEA FUMAC project. Presented at the OECD/NEA Expert Group on Reactor Fuel Performance (EGRFP), Paris, France, February 16, 2016.

[34] K. Kulacsy. Communication within the IAEA Fuel Modelling under Accident Conditions (FUMAC) Project, 2015.